

Peptidic Monodisperse PEG “Comb” as Multifunctional “Add-On” Module for Imaging-Traceable and Thermo-Responsive Theranostics

Junfei Zhu, Huaibin Zhang, Kexin Chen, Yu Li, Zhigang Yang, Shizhen Chen, Xing Zheng, Xin Zhou, and Zhong-Xing Jiang*

Monodisperse polyethylene glycols–modified (M-PEGylated) biomaterials exhibit high structural accuracy, biocompatibility, and fine-tunable physico-chemical properties. To develop “smart” drug delivery systems in a controllable and convenient manner, a peptidic M-PEG “comb” with fluorinated *L*-lysine side chains and a fluorescent *N*-terminal is conveniently prepared as a ^{19}F magnetic resonance imaging (^{19}F MRI) and fluorescence dual-imaging traceable and thermo-responsive “add-on” module for liposomal theranostics in cancer therapy. The peptidic M-PEG “comb” has high biocompatibility, thermo-responsivity with a sharp lower critical solution temperature, an aggregation-induced emission fluorescence, and high ^{19}F MRI sensitivity. As a highly branched amphiphile, it self-assembles and firmly anchors on the doxorubicin-loaded liposomal nanoparticles, which M-PEGylates the liposomes and facilitates the thermo-responsive drug release and drug tracking with dual-imaging technologies. In a rodent xenograft model of human liver cancer HepG2 cells, the M-PEGylated liposomes exhibit long in vivo half time, low toxicity, high tumor accumulation, “hot spot” ^{19}F MRI, and therapeutic efficacy. With accurately programmable chemical structure, fine-tunable physicochemical and biological properties to meet the demands of diagnosis, drug delivery, and therapy, the M-PEG “comb” is promising as a versatile “add-on” module for rapid and convenient formulation of various “smart” theranostics.

1. Introduction

As the most used polymers in biomedicine, the extraordinary properties of polyethylene glycols (PEGs), such as high biocompatibility, “stealthy effect” to immune system and proteases, high solubility in both water and organic solvents, et. al., have been regarded as the “gold standards” for biomaterials.^[1] Since the 1970s, PEGs have been extensively used as versatile linkers in various bioconjugates, solubility and biocompatibility enhancers in formulation, “bio-shield” to reduce immune response, renal excretion, and degradation in biopharmaceuticals, etc. PEGylation has become one of the most successful drug development strategies in pharmaceutical industry, especially in the R&D of biopharmaceuticals and nanomedicine.^[2] Till 2015, 17 PEGylated drugs had been approved by U.S. Food and Drug Administration, including 15 biopharmaceuticals, 1 small molecular drug, and 1 nanomedicine (liposomal doxorubicin, Caelyx). However, as complex homolog

Dr. J. Zhu, H. Zhang, Prof. Z. Yang, Prof. Z.-X. Jiang
Hubei Province Engineering and Technology
Research Center for Fluorinated Pharmaceuticals
School of Pharmaceutical Sciences
Wuhan University
Wuhan 430071, China
E-mail: zxjiang@whu.edu.cn

H. Zhang, Dr. Y. Li, Prof. S. Chen, Prof. X. Zhou
State Key Laboratory for Magnetic Resonance and Atomic
and Molecular Physics
National Center for Magnetic Resonance in Wuhan
Wuhan Institute of Physics and Mathematics
Chinese Academy of Sciences
Wuhan 430071, China

K. Chen, Prof. X. Zheng
Group of Lead Compound
Institute of Pharmacy & Pharmacology
Hunan Province Cooperative Innovation Center
for Molecular Target New Drug Study
University of South China
Hengyang 421001, China

 The ORCID identification number(s) for the author(s) of this article can be found under <https://doi.org/10.1002/adhm.201901331>.

DOI: 10.1002/adhm.201901331

mixtures, the polydispersity of regular PEGs complicates their biomedical applications by introducing uncertainties and difficulties during PEGylation, purification, quality control, regulatory approval, etc.^[3] Although the issues accompanied by polydisperse PEGs are obvious, they are overwhelmingly used in biomedicine because it is challenging to synthesize their monodisperse counterparts.^[4]

PEGylated liposomal drug delivery systems with multimodal imaging and stimuli-responsive property are highly valuable theranostics.^[5] First, comparing to their non-PEGylated counterparts, PEGylated liposomes, with Caelyx as an example, usually exhibit extended in vivo half time, reduced toxicity, improved “passive” targeting, and therapeutic efficacy.^[2] Second, multimodal imaging can not only facilitate tracking of the liposomal drug delivery system, but also provide valuable information about the local pathological environment and therapeutic response, which yields theranostics for optimal therapeutic efficacy.^[6] Third, stimuli-responsive liposomes are capable of releasing the encapsulated drug at the target in a controllable and targeted way, which further maximizes the therapeutic efficacy and minimizes the side effects.^[7] However, it is very tedious and challenging to integrate multiple components of diverse physicochemical properties and functions, e.g., PEGylation agent, multiple imaging agents, stimuli-responsive materials, drug, surfactant, etc., into stable liposomal theranostics. Indeed, stimuli-responsive liposomes usually suffer the complexity, toxicity, biodegradability, and scale-up ability

of stimuli-responsive materials, such as proteins, block copolymers, and dendrimers.^[8] In addition, it is difficult to spatially and temporally synchronize the imaging agents with the drugs in an accurate, real-time, and quantitative way because of their heterogenous distribution among the liposomal nanoparticles and immature release of the imaging agents and drugs. Therefore, it would be beneficial to integrate the multiple liposomal components of different functions, such as PEGylation, dual imaging modalities, stimuli-responsive property, etc., into a versatile “add-on” module for the construction of liposomal theranostics with multimodal imaging and stimuli-responsive capabilities.

Recently, a macrocyclic sulfate-based strategy for the convenient synthesis of M-PEGs and their derivatives was developed in this group and it was found that replacing the polydisperse PEGs with M-PEGs in biomedical research is highly beneficial for quantitatively optimizing solubility, biocompatibility, biodegradability, drug efficacy and safety, and imaging properties.^[9] Notably, M-PEGylated amphiphilic peptides were promising imaging-traceable and thermo-responsive biomaterials.^[6b] Herein, we programed the chemical structure of the M-PEGylated peptides into peptidic M-PEG “comb” 1 as an “add-on” module with sensitive ¹⁹F MRI (magnetic resonance imaging)/fluorescence dual imaging and thermo-sensitivity for the convenient construction of multifunctional “smart” liposomal theranostics (Figure 1). Thanks to the versatile peptide chemistry, the chemical structure, physicochemical

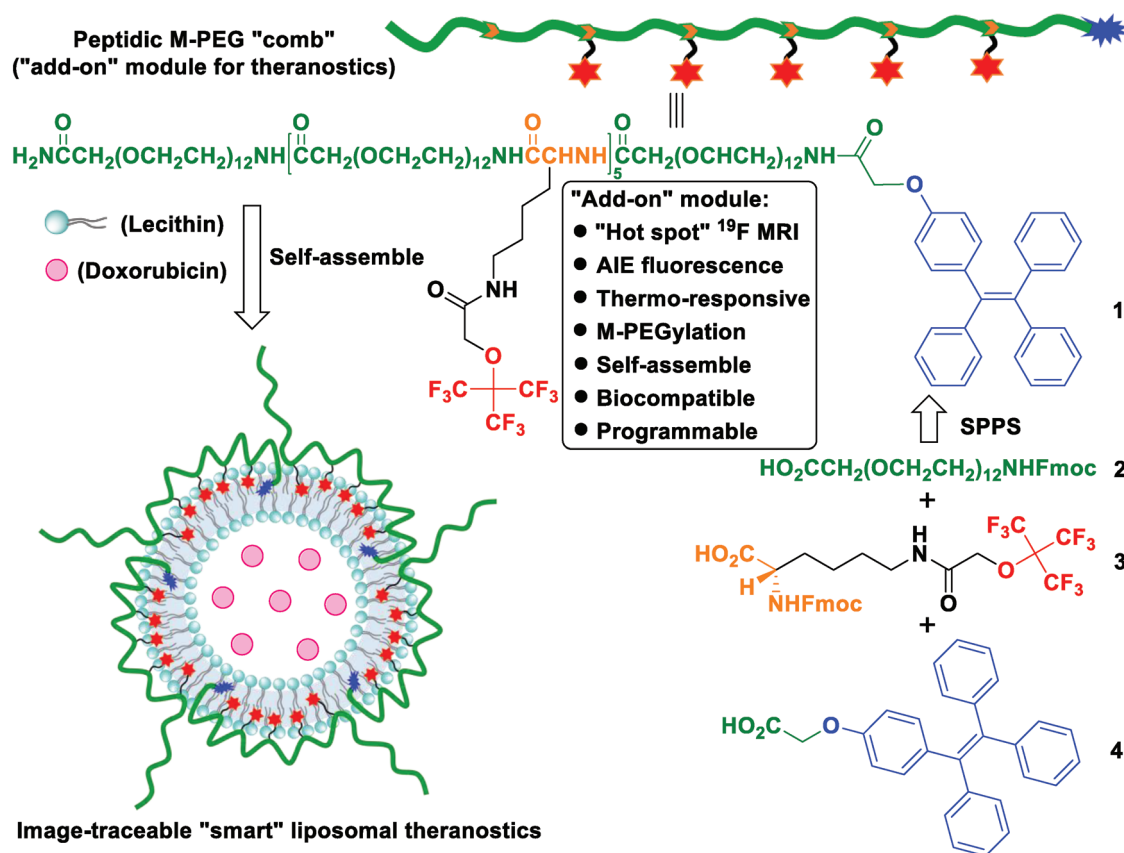


Figure 1. The design of peptidic M-PEG “comb” 1 as “add-on” module for liposomal theranostics.

and biological properties of the “add-on” module can be accurately programmed for potential biomedical applications.^[68,9c] In this case, ¹⁹F MRI and fluorescent imaging were incorporated into the “add-on” module because they complement each other by taking the advantage of no tissue depth limit, no ionizing radiation, “hot spot” in vivo image of ¹⁹F MRI, and high sensitivity and convenience in vitro images of fluorescence. Structurally, the peptidic backbone of M-PEG “comb” **1** was composed of M-PEG-containing ω -amino acid **2** and fluorinated *L*-lysine **3**, which *N*-terminal was capped with a tetraphenylethene-containing acid **4**. In this way, 45 fluorines on the lysine side chains have similar chemical environments and accumulatively give a strong signal for sensitive ¹⁹F MRI. When formulate into liposomal theranostics, the hydrophobic interaction between the five fluorinated *L*-lysine sidechains and the lipid bilayer would facilitate the firm anchoring of M-PEG “comb” **1** on the liposomal nanoparticle surface, while the M-PEG fragments would PEGylate the nanoparticle and therefore enhance the biocompatibility and in vivo half-time of the liposomes. A dodecaethylene glycol fragment was chosen as the backbone of ω -amino acid **2** because much higher biocompatibility was found for peptidic M-PEGs containing relatively long PEG fragments in our previous study.^[68] Tetraphenylethene with aggregation-induced emission (AIE) fluorescence was introduced as a “smart” fluorophore to trace the liposomes in vitro and monitor the self-assembly of M-PEG “comb” **1**. According to our previous study,^[68,10] such amphiphilic M-PEG “combs” would exhibit thermo-responsive property and a sharp lower critical solution temperature (LCST) around body temperature, which may trigger drug release at “hot” regions, like tumor and inflammatory tissues. As an “add-on” module, M-PEG “comb” **1** along with its multimodal imaging and thermo-responsive property can be easily introduced into various liposomes through self-assembly, which provides a convenient and general strategy for multimodal image traceable and multi-functional

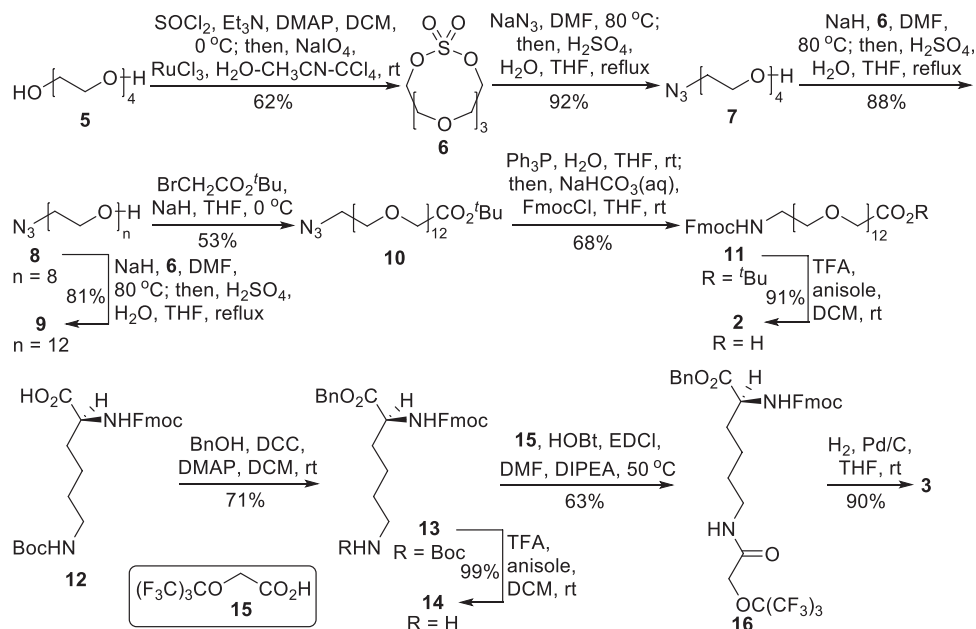
theranostics. In this study, anticancer drug, doxorubicin, was loaded in the liposomal theranostics for cancer therapy.

2. Results and Discussion

2.1. Synthesis, Physicochemical Property, and Biocompatibility of M-PEG “Comb” **1**

The synthesis of M-PEG “comb” **1** was commenced with the construction of ω -amino acid **2** and *L*-lysine derivative **3** (Scheme 1). Through a macrocyclic sulfate-based strategy, Fmoc-protected ω -amino acid **2** was conveniently prepared from tetraethylene glycol **5** with the selective ring opening reaction of macrocyclic sulfate **6** as the key steps on a 10 g scale. From commercially available Fmoc- and Boc-protected *L*-lysine **12**, fluorinated *L*-lysine derivative **3** was prepared on a 3 g scale in four steps with an overall yield of 40%. The fluorinated acid **15** was conveniently prepared from perfluoro-*tert*-butanol and tetraphenylethene derivative **4** was prepared according to a reported method (see the Supporting Information). With amino acids **2**, **3**, and tetraphenylethene derivative **4** in hand, M-PEG “comb” **1** were then prepared through Fmoc-strategy solid-phase peptide synthesis on a multi-hundred milligram scale with high purity and full characterization (see the Supporting Information).

With peptidic M-PEG “comb” **1** in hand, its physicochemical and biological properties were then investigated. First, M-PEG “comb” **1** was freely soluble in water because of the seven highly hydrophilic M-PEG fragments on the peptidic backbone. Second, M-PEG “comb” **1** showed a strong UV absorption with a maximum absorption at 310 nm and a strong fluorescent emission at 470 nm (Figure 2a,b). When increasing the concentration of M-PEG “comb” **1** in water, a concentration-dependent fluorescent emission and redshift of the UV



Scheme 1. Synthesis of amino acids **2** and **3**.

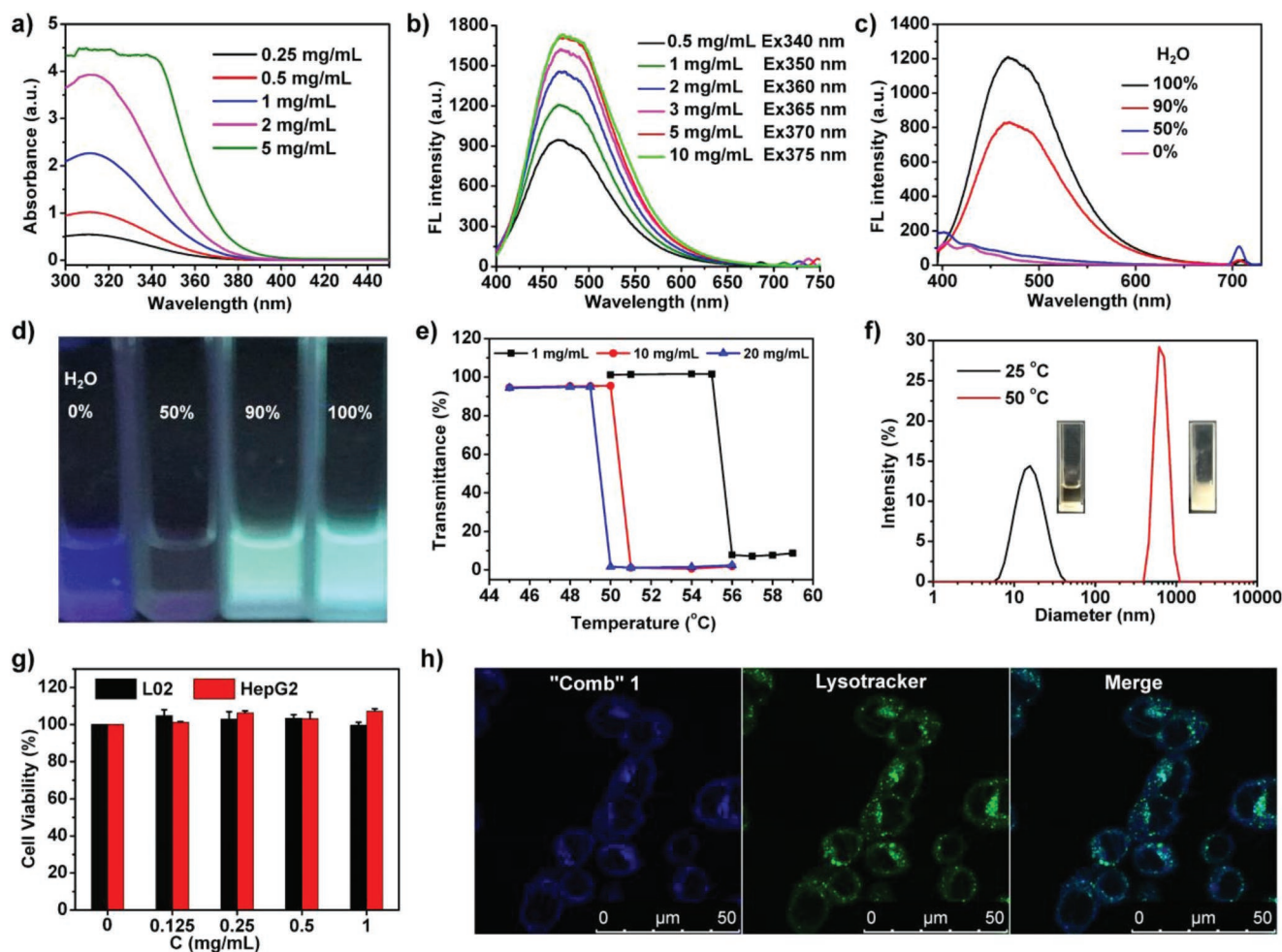


Figure 2. a) Concentration-dependent UV absorption and b) fluorescent emission, solvent-induced AIE fluorescent emission c) curves and d) images, e) turbidity curves (concentration as indicated), f) DLS (concentration = 1.53×10^{-3} M, with the corresponding inserted images of the solution), g) cell viability assay (in L02 cells and HepG2 cells), and h) confocal images (left at 30×10^{-6} M of module 1, center at 200×10^{-9} M of lysotracker, right overlay of two images, in HepG2 cells after 2 h) of module 1. Data were presented as mean \pm standard deviation ($n = 3$).

absorption were observed. When switching the solvent from methanol to water, M-PEG “comb” 1 exhibited strong AIE fluorescence, which indicated the hydrophobic interaction and π - π stacking as the driving forces for the self-assembly in water (Figure 2c,d). Third, as expected, a sharp LCST of 49 °C was detected from the turbidity curves of M-PEG “comb” 1 at 20 mg mL⁻¹ (Figure 2e). The LCST was concentration-dependent, i.e., the higher the concentration the lower LCST, which was in consistent with our previous study.^[6] With the aid of dynamic light scattering (DLS), a dramatic particle size expansion from 15 to 656 nm was observed when heating the M-PEG “comb” 1 solution from clear to turbid (Figure 2f), which showed the temperature-dependent self-assembly profiles of M-PEG “comb” 1. Finally, the biocompatibility and cell permeability of M-PEG “comb” 1 were investigated. The biocompatibility of PEGylated perfluoro-*tert*-butanol and perfluoropinacol heavily depends on the molecular geometry: many linear ones are highly toxic,^[11] while many branched ones are highly biocompatible.^[6d,g,9a,12] Here, high biocompatibility of M-PEG “comb” 1 was observed during the cell viability assays in human hepatic cell line, L02

cells, and human liver cancer cell line, HepG2 cells (Figure 2g). Furthermore, it is noteworthy that no acute toxicity was found when M-PEG “comb” 1 was injected into Balb/c mice through tail vein at a high dose of 1.5 g kg⁻¹. Based on previous reports and the findings here, the highly branched “comb” structure and the relatively long dodecaethylene glycol fragments of M-PEG “comb” 1 may contribute to its high biocompatibility. Confocal microscopic images showed that M-PEG “comb” 1 can cross HepG2 cell membrane and enter cells through lysosome (Figure 2h).

Then, ¹⁹F MRI properties of peptidic M-PEG “comb” 1 were investigated. In methanol, M-PEG “comb” 1 gave a sharp and singlet ¹⁹F NMR peak from its 45 fluorines (Figure 3a, top). When switching the solvent from methanol to water, five peaks were detected from its ¹⁹F NMR spectrum (Figure 3a, bottom). The ¹⁹F NMR signal splitting of PEG “comb” 1 in water showed the formation of self-assemble nanoparticles in water in which the five fluorinated *L*-lysine sidechains were in different chemical environment. Fortunately, the five ¹⁹F NMR peaks of M-PEG “comb” 1 were close enough for accumulatively generating

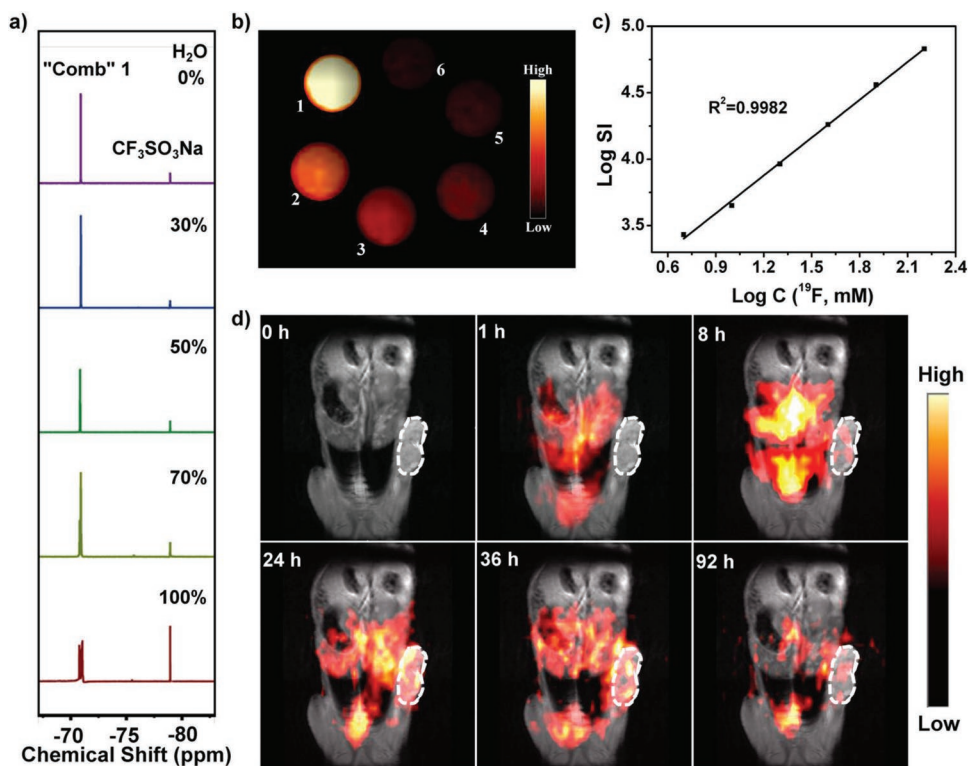


Figure 3. a) Solvent-dependent ^{19}F NMR (top: 100% MeOH, bottom: 100% water, $\text{CF}_3\text{SO}_3\text{Na}$ as internal standard) and b) ^{19}F MRI phantom images (concentrations from 1 to 6 are 3.5×10^{-3} , 1.8×10^{-3} , 0.89×10^{-3} , 0.44×10^{-3} , 0.22×10^{-3} , 0.11×10^{-3} M in water) of module 1, c) plot of $\log \text{SI}(^{19}\text{F})$ versus $\log C(1)$ ($\text{SI} = ^{19}\text{F}$ MRI signal intensity), and d) time-dependent in vivo ^{19}F MRI images of mice carrying HepG2 tumor after tail vein injection of module 1 ($n = 3$).

sensitive ^{19}F MRI (Figure 3b). The relatively short ^{19}F relaxation times of M-PEG “comb” 1 ($T_1 = 542$ ms, $T_2 = 152$ ms, 1.53×10^{-3} M in water, 25°C) also contributed to the high ^{19}F MRI sensitivity by shortening the data collection time. As expected, a low ^{19}F MRI detectable concentration of 0.11×10^{-3} M was found for M-PEG “comb” 1 during the phantom experiments, which was close to many in vivo drug concentrations. It was noteworthy that M-PEG “comb” 1 concentration was proportional to its ^{19}F MRI signal intensity (Figure 3c), which would be valuable for quantitatively tracking M-PEG “comb” 1 and its nanoparticles with ^{19}F MRI. Then, an in vivo ^{19}F MRI study was carried out in a xenograft tumor model of HepG2 cells in three nude mice (Figure 3d). After tail vein injection of M-PEG “comb” 1 at $0.23 \text{ mmol kg}^{-1}$, ^{19}F MRI images were obtained at a series of time points. It was found that M-PEG “comb” 1 can be traced in vivo with ^{19}F MRI even 92 h after the injection, which showed its relatively long in vivo retention time in mice. It was very interesting to point out that M-PEG “comb” 1 would accumulate in tumor and provide the “hot spot” ^{19}F MRI images of tumor.

2.2. Formulation of Theranostics with the “Add-On” Module

Based on the above results, M-PEG “comb” 1 was employed as an “add-on” module for the construction of liposomal theranostics with ^{19}F MRI and fluorescent dual-imaging as well as thermo-sensitive drug release. When lecithin and M-PEG

“comb” 1 were formulated with a film dispersion method, liposomes **L0** with a particle size of 96.3 nm and a polydispersity index (PDI) of 0.187 were obtained (Figure 4a,b). Using a pH gradient strategy, anticancer drug doxorubicin (DOX·HCl) was loaded into liposomes **L0** to give liposomes **L1** with a particle size of 70.6 nm, a PDI of 0.169, and a drug entrapment efficiency of 95% (Figure 4a,c). The DOX-loaded liposomes **L1** were found to be stable when stored at room temperature over 30 days or in Dulbecco’s modified Eagle medium (DMEM) medium containing 10% fetal bovine serum (FBS) over 4 days (Figure 4d). It was noteworthy that the nanoemulsions formulated by directly loading DOX with M-PEG “comb” 1 suffered low DOX loading efficacy and emulsion stability. As a result of thermo-responsive M-PEG “comb” 1 on the liposomal nanoparticles, liposomes **L1** released DOX much faster at 42°C than body temperature (Figure 4e), which showed the potential of **L1** in cancer and inflammation diseases-targeted drug delivery. Liposomes **L1** also showed comparable or slightly higher cytotoxicity than DOX toward HepG2 cells (Figure 4f). Liposomes **L1** showed valuable dual-imaging modalities. On one hand, liposomes **L1** emitted strong fluorescence from both M-PEG “comb” 1 and DOX, which facilitated cellular study. With the aids of confocal microscopy and lysotracker, fluorescent images indicated that liposomes **L1** can cross HepG2 cell membrane and deliver DOX into cells through lysosome (Figure 4g). On the other hand, liposomes **L1** showed a strong ^{19}F NMR signal and high ^{19}F MRI sensitivity (Figure S1, Supporting Information), which may be used to trace the drug delivery system in

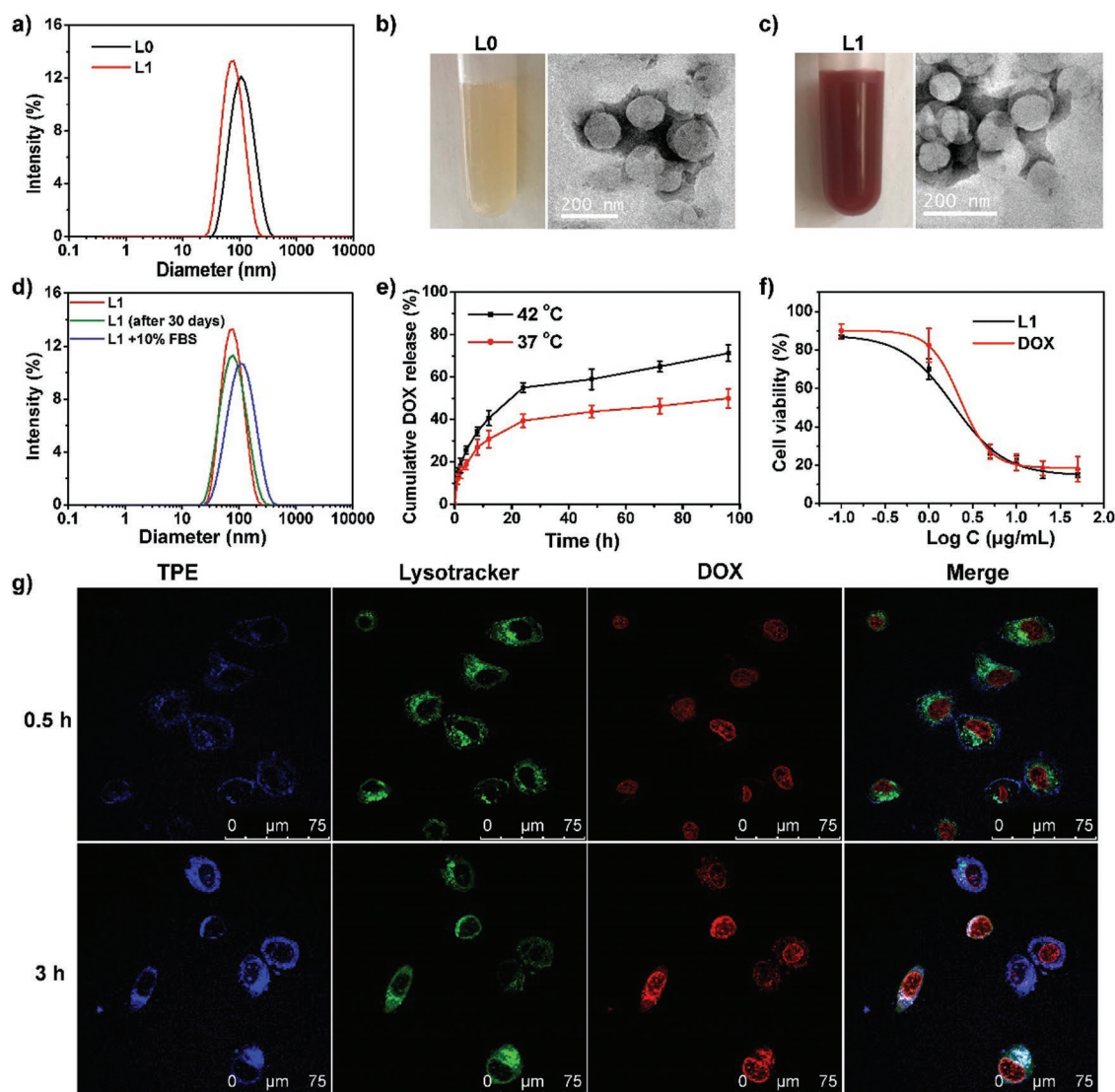


Figure 4. a) DLS, b,c) photos (with insertion of TEM images), and d) stability study with DLS of liposomes L0 and L1, e) temperature-dependent drug release curves, f) cytotoxicity assays, and g) confocal images of liposomes L1. Data were presented as mean \pm standard deviation ($n = 3$).

deep tissues. The high stability, cytotoxicity, thermo-sensitivity, and dual-imaging modality made liposomes L1 a promising theranostics.

2.3. Cancer Therapy with the Theranostics

With the multifunctional theranostics L1 in hand, an image-guided cancer therapy was carried out in nude mice xenograft tumor model of HepG2 cells. First, at a very low dose of $0.077 \text{ mmol kg}^{-1}$, the liposomal theranostics L1 can be traced in vivo with “hot spot” ^{19}F MRI which showed not only the biodistribution of theranostics L1 in mice, but also its aggregation in tumor region as a result of the enhanced permeability and retention effect of the nanoparticles (Figure 5a). Comparing to the literatures of in vivo drug-tracking with ^{19}F MRI,^[13] the imaging agent dosage here is the lowest. The “hot spot” in vivo tracking of theranostics L1 with ^{19}F MRI in

mice was also illustrated by the ^{19}F MRI images of a mouse after intratumoral injection of theranostics L1 (Figure 5b). The aggregation of theranostics L1 in tumor was confirmed by analyzing the tissue concentration of M-PEG “comb” 1 and DOX in major internal organs at the 12th h after intravenous (iv) injection (Figure 5c). Second, in vivo pharmacokinetics study indicated that the mice injected with theranostics 1 had higher plasma DOX concentration than that of mice injected with DOX (Figure 5d), which may be valuable for maintain high in vivo drug level and reducing the dosing frequency. According to Figure 5d, the half-life time of DOX and theranostics L1 in plasma were calculated as < 5 and ≈ 15 min, respectively. Third, a therapeutic efficacy study was carried out on three groups of tumor-carrying mice with five mice in each group, in which the three groups of mice were injected through tail vein with saline, DOX, or theranostics L1, respectively. Considerable tumor growth inhibition was observed in the groups treated with DOX and theranostics L1 (Figure 5e,g). Importantly, the

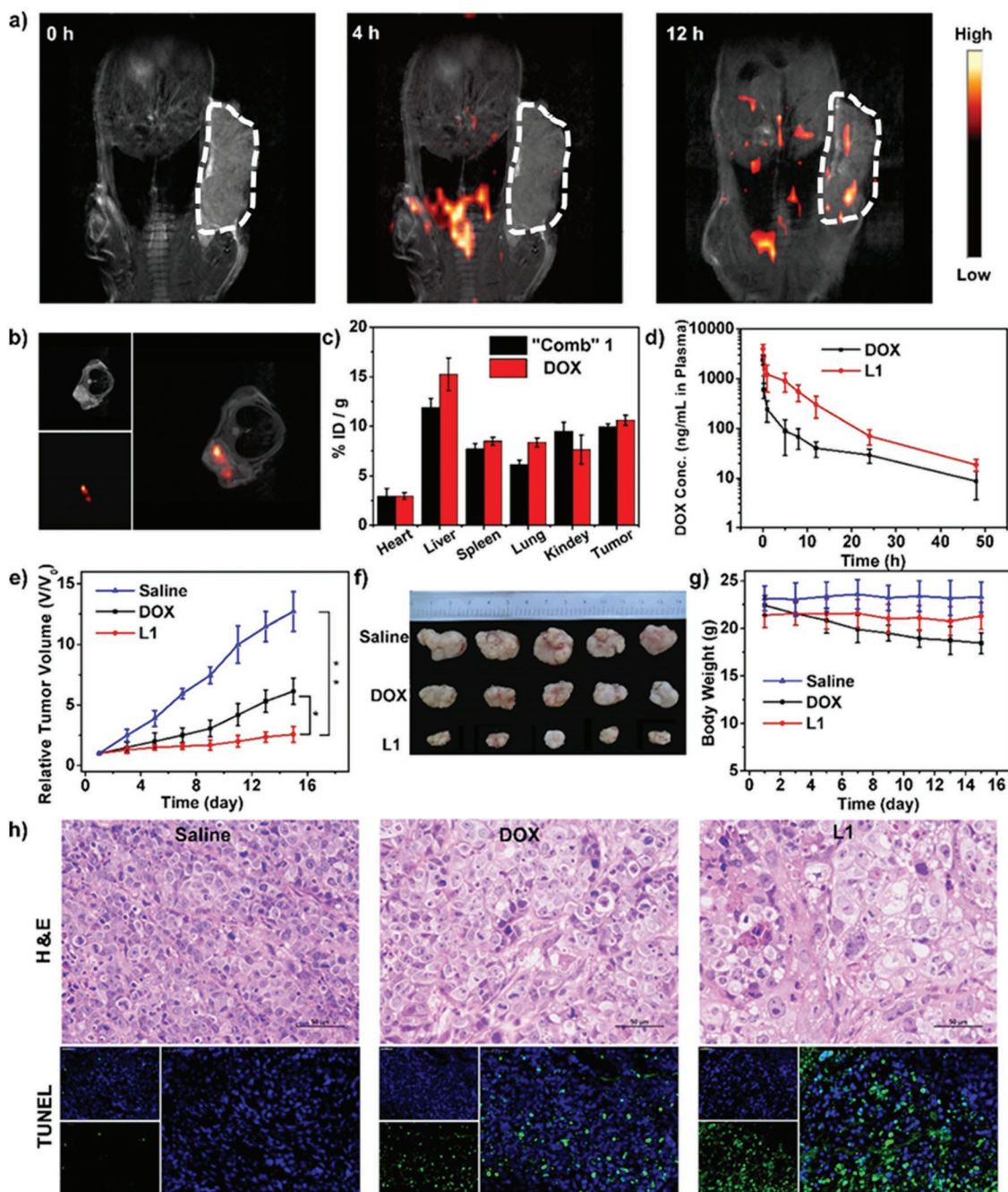


Figure 5. a) ^{19}F MRI images of mouse after tail vein injection and b) tumor after intratumoral injection of theranostics L1, c) M-PEG “comb” 1 and DOX concentration in major organs at 12 h post the tail vein inject of theranostics L1, d) plasma concentration of DOX after tail vein injection of theranostics L1 or DOX (5 mg kg^{-1}), e) tumor growth curves, f) photos of tumor size comparison, and g) mice body weight curves of the three treatment groups dosed with saline, DOX, and theranostics L1, h) H&E and TUNEL staining of HepG2 tumor tissues from the three treatment groups. Data were presented as mean \pm standard deviation ($n = 3$ for (a)–(d), $n = 5$ for (e)–(g)); the asterisks indicate the differences between L1 and the other groups, $*p < 0.05$, and $**p < 0.01$.

sizes of tumor in the theranostics L1 treated group were much smaller than that of the DOX treated group, which showed the improved therapeutic efficacy of theranostics L1 (Figure 5e,g). Body weigh comparison of the three treatment groups during the study showed much lower toxicity of liposomes L1 than DOX (Figure 5f). Finally, the hematoxylin and eosin (H&E) and TUNEL (terminal deoxynucleotidyl transferase dUTP nick end

labeling) staining of mice tissues showed that theranostics L1 were more efficacious in depleted tumor cells and less toxic to normal tissue than DOX (Figure 5h and Figure S3, Supporting Information). Therefore, with the “add-on” module, theranostics L1 could not only provide in vivo “hot spot” ^{19}F MRI images, but also improve the therapeutic efficacy and lower the toxicity.

3. Conclusion and Outlook

In this study, we have developed a dual-image-traceable and thermo-responsive M-PEG “comb” as a general and multi-functional “add-on” module for the convenient construction of “smart” liposomal theranostics in cancer therapy. The imaging-guided cancer therapy with the liposomal theranostics has been demonstrated in both cancer cell lines and murine xenograft tumor model. The ^{19}F MRI/fluorescence dual-imaging provided valuable *in vitro* and *in vivo* drug and tumor images. Significantly higher therapeutic efficacy and overall survival of animal was found for the M-PEG “comb”-containing theranostics. In recent years, a large number of drug delivery systems, including many theranostics, have been developed, which brought tremendous new ideals for fighting against challenging diseases. However, most of these systems have too much complexity, but not enough reproducibility,^[14] which significantly hampered their clinical application. So, it would be highly valuable to develop drug delivery systems in a simple and accurate way. The “add-on” modular strategy developed here is aimed to relieve the complexity in liposomal theranostics. First, the M-PEG “comb” is a monodisperse peptide with accurate chemical structure which completely avoids the heterogeneity issues in such overwhelmingly used polydisperse biomaterials, as PEGs, polyethyleneimine, poly(lactic-co-glycolic acid), poly lactic acid, poly glycolic acid, etc. Moreover, the structure of the peptidic M-PEG “combs” can be accurately programmed on solid-phase peptide synthesis, which enables the fine tuning of their physicochemical and biological properties. Second, a general and versatile “add-on” module can not only simplify the drug delivery system by replacing multiple components, such as ^{19}F MRI agents, fluorophore, PEGylation agents, and thermo-responsive biomaterials, et al., with just one module, but also provide a general strategy for the convenient construction of drug-loaded thermo-responsive theranostics with M-PEGylation, “hot spot” ^{19}F MRI and convenient fluorescence dual-imaging. Meanwhile, replacing multiple components with one monodisperse module reduces the uncertainties during formulation and application of the theranostics. Third, in terms of PEGylation, the peptidic M-PEG “comb” successfully avoided two major drawbacks of regular linear polydisperse PEGylation agents: polydisperse and nonbiodegradable. The M-PEG “comb” is monodisperse and its biodegradable amide bonds would promote its degradation to M-PEGs-containing amino acids and natural amino acids. Currently, the modular strategy has been extensively used in information technology, science, and engineering and its great success has been proved by the rapid changes of our daily lives. Therefore, in a similar way, the application of modular strategies in biomedicine may simplify, standardize, promote biomedical R&D in a controllable and precise manner.

4. Experimental Section

Cell Culture and Cytotoxicity Assay: L02 and HepG2 cells were cultured in DMEM medium containing 10% FBS. All cells were cultured at 37 °C in humidified atmosphere containing 5% CO_2 and the growth medium was replaced with fresh media every 24 h. The biocompatibility assay of the M-PEGs peptides was evaluated by 3-(4,5-dimethylthiazol-2-yl)-2,5-diphenyltetrazolium bromide (MTT) assays. For the biocompatibility assay, L02 and HepG2 cells were seeded into a 96-well plate and allowed

for adherent culture at 37 °C for several hours. Subsequently, a gradient concentration of “comb” 1 ranging from 125 to 1000 $\mu\text{g mL}^{-1}$ was added in a series of wells. Every concentration was set with five wells at least. The wells with 100 μL culture medium alone were used as negative control and wells containing cells alone were used as positive control. After incubation for 24 h, the medium was replaced with 100 μL MTT (1.0 mg mL^{-1}) solution and incubated for 4 h. Then the medium was replaced with 100 μL dimethyl sulfoxide and the absorbance value was measured at 490 nm using a microplate reader. All of the experiments were repeated three times at least. Antiproliferation efficiency of L1 and DOX on HepG2 cells was performed with MTT assay in the similar fashion.

Intracellular Distribution Analysis of “Comb” 1 and L1: After seeding HepG2 cells in confocal dishes and culturing for 24 h, “comb” 1 (200 $\mu\text{g mL}^{-1}$) was added and the cells were incubated at 37 °C for 2 h. Then, the supernatant was carefully removed and the cells were rinsed with phosphate-buffered saline buffer twice. After staining with LysoTracker Green DND-26 (5000 times dilution in DMEM) for 20 min at 37 °C, cells were rinsed with DMEM twice and imaged using a confocal laser scanning microscopy (Leica-LCS-SP8-STED). Intracellular distribution analysis of L1 on HepG2 cells were imaged with confocal laser scanning microscopy in the similar fashion after incubation at 37 °C for 0.5 and 3 h.

Mice ^{19}F MRI Experiments: Mice ^{19}F MRI Experiment of “comb” 1: 200 μL of “comb” 1 solution (in deionized water, ^{19}F dose was 10 mmol kg^{-1}) was intravenously injected into the HepG2 tumor-bearing mice. ^1H MRI and ^{19}F MRI for each mouse were collected over time (at 0, 1, 4, 8, 24, 34, 58, 92 h) on a 400 MHz Bruker BioSpec MRI system after the injection with isoflurane as anesthetics. ^1H MRI: method = RARE-T₁, matrix size = 256 × 256, FOV (field of view) = 4/3 cm, time of repetition (TR) = 3000 ms, time of echo (TE) = 22 ms, slice thickness (SI) = 2/2 cm, scan time = 576 s; ^{19}F MRI: method = RARE, matrix size = 32 × 32, FOV = 5/3.75 cm, SI = 15 mm, TR = 1500 ms, TE = 3 ms, scan time = 1536 s.

Mice ^{19}F MRI Experiment of L1: 150 μL of L1 solution (^{19}F dose was 5 mmol kg^{-1}) was intravenously injected into the HepG2 tumor-bearing mice. ^1H MRI and ^{19}F MRI for each mouse were collected over time (at 0, 4, 12, 24 h) on a 400 MHz Bruker BioSpec MRI system after the injection with 1% pentobarbital sodium as anesthetics. ^1H MRI: method = RARE-T₁, matrix size = 256 × 256, FOV = 4/3 cm, TR = 2500 ms, TE = 33 ms, SI = 2/2 cm, scan time = 80 s; ^{19}F MRI: method = RARE, matrix size = 32 × 32, FOV = 5/3.7 cm, SI = 27.2 mm, TR = 1500 ms, TE = 3 ms, scan time = 1536 s.

In Vivo Pharmacokinetic (PK) Study of Free and Encapsulated Drugs: For the PK assay, male Balb/c mice (6 mice per group) were injected with free DOX, or liposomes L1 (at an equivalent dose of 5 mg kg^{-1} DOX) through the tail vein. Three mice were randomly chosen for the first four time points, and the other three mice were used for the remaining four time points. Approximately 100 μL of blood was collected in 0.5 mL heparin-treated tubes from the orbit sinus at each time point (0.083, 0.25, 1, 5, 8, 12, 24, 48 h). The blood samples were extracted with chloroform/MeOH (4:1, 2 mL) and centrifuged at 3000 rpm for 10 min. The lower organic phase was concentrated and dried, and then dissolved with 50 μL methanol. The samples were oscillated for 3 min, sonicated for 2 min, and centrifuged at 4000 rpm for 5 min. The supernatant was collected and determined by high-performance liquid chromatography (HPLC) analysis. The chromatographic conditions were as follows: SPD-20A UV detector (480 nm), a Sunfire C18 column (5 μm , 4.6 × 100 mm), a gradient elution of solvent A (ammonium dihydrogen phosphate buffer, water containing 0.5% v/v acetic acid and 0.01 M of ammonium dihydrogen phosphate, 0.35 mL min^{-1}) and solvent B (MeOH, 0.35 mL min^{-1}).

Assessment of the Biodistribution of L1: The HepG2 tumor-bearing nude mice were injected with 100 μL of liposomes L1 at an equivalent dose of 5 mg kg^{-1} DOX via tail vein ($n = 3$). At 12 h after iv injection, the mice were euthanized and the heart, liver, spleen, lung, kidney, and tumor were collected. After tissue homogenization and lyophilization, DOX and “comb” 1 in tissue samples were extracted with chloroform/MeOH (4:1). The organic phase was concentrated and dried, and then dissolved in 200 μL methanol. Then the concentration of DOX and “comb” 1 were determined by HPLC, respectively. The concentration of DOX and “comb” 1 were expressed as percentage of injected dose per

gram tissue (% ID per g tissue). For “comb” 1 HPLC analysis: SPD-20A UV detector (330 nm), a Sunfire C18 column (5 μ m, 4.6 \times 100 mm), gradient elution sequence: i) 75% to 85% MeOH in water, 0–10 min; ii) 85% to 100% MeOH in water, 10–25 min, flow rate 1 mL min⁻¹. For DOX HPLC analysis: SPD-20A UV detector (480 nm), a Sunfire C18 column (5 μ m, 4.6 \times 100 mm), a gradient elution of solvent A (ammonium dihydrogen phosphate buffer, water containing 0.5% v/v acetic acid and 0.01 M of ammonium dihydrogen phosphate, 0.15 mL min⁻¹) and solvent B (MeOH, 0.15 mL min⁻¹).

Tumor Growth Inhibition using Liposomes L1: The HepG2 tumor-bearing nude mice were randomly assigned to three groups (five animals each) at this stage when the tumor sizes approached 100–150 mm³. The mice were intravenously injected with saline (100 μ L), free DOX (100 μ L, 5 mg kg⁻¹), or liposomes L1 (100 μ L, at an equivalent dose of 5 mg kg⁻¹ DOX) at the time points of 1, 4, and 7 days, respectively. The tumor volume and body weight of the mice were measured every 2 days. Tumor volume was measured with a vernier caliper and calculated using the following equation: volume = 0.5 \times L \times W², where “W” and “L” represent the width and length of the tumor, respectively. The relative tumor volume was calculated as V/V₀ (V₀ was the tumor volume before injection). On the 14th day, all the mice were sacrificed and the tumor tissues were excised and collected for immunofluorescence and immunohistochemistry analysis. The animal experimental procedures were performed in accordance with the National Institutes of Health Guide for the Care and Use of Laboratory Animals and were approved by the local Animal Care and Use Committee.

Statistics: Results were expressed as means \pm SD of three independent experiments. Significance in Figure 5e was determined via one-way analysis of variance compared to the sample's respective prestim value. Statistical significance was denoted by **p* < 0.05, ***p* < 0.01, and ****p* < 0.001. Statistical analysis was performed in OriginLab OriginPro 8.5.

Supporting Information

Supporting Information is available from the Wiley Online Library or from the author.

Acknowledgements

The authors are thankful for the financial support from the National Key R&D Program of China (2016YFC1304704, 2018YFA0704000), the National Natural Science Foundation of China (21572168, and 81625011), and the Key Research Program of Frontier Sciences, CAS (QYZDY-SSW-SLH018).

Conflict of Interest

The authors declare no conflict of interest.

Keywords

drug delivery, imaging, liposome, polyethylene glycols, stimuli-responsive biomaterials

Received: September 19, 2019

Revised: November 14, 2019

Published online: December 18, 2019

- [1] a) J. M. Harris, R. B. Chess, *Nat. Rev. Drug Discovery* **2003**, *2*, 214; b) K. Knop, R. Hoogenboom, D. Fischer, U. S. Schubert, *Angew. Chem., Int. Ed.* **2010**, *49*, 6288; c) M. C. Parrott, J. M. DeSimone,

Nat. Chem. **2012**, *4*, 13; d) J. Herzberger, K. Niederer, H. Pohlitz, J. Seiwert, M. Worm, F. R. Wurm, H. Frey, *Chem. Rev.* **2016**, *116*, 2170; e) J. Cui, M. Björnalm, Y. Ju, F. Caruso, *Langmuir* **2018**, *34*, 10817.

- [2] a) F. M. Veronese, G. Pasut, *Drug Discovery Today* **2005**, *10*, 1451; b) F. M. Veronese, A. Mero, *BioDrugs* **2008**, *22*, 315; c) C. S. Fishburn, *J. Pharm. Sci.* **2008**, *97*, 4167; d) J. S. Suk, Q. Xu, N. Kim, J. Hanes, L. M. Ensign, *Adv. Drug Delivery Rev.* **2016**, *99*, 28.
- [3] a) A. P. Chapman, P. Antoniwi, M. Spitali, S. West, S. Stephens, D. J. King, *Nat. Biotechnol.* **1999**, *17*, 780; b) J. E. Seely, C. W. Richey, *J. Chromatogr. A* **2001**, *908*, 235; c) R. Haag, F. Kratz, *Angew. Chem., Int. Ed.* **2006**, *45*, 1198; d) C. J. Fee, J. M. Van Alstine, *Chem. Eng. Sci.* **2006**, *61*, 924; e) M. J. Vicent, L. Dieudonné, R. J. Carbajo, A. Pineda-Lucena, *Expert Opin. Drug Delivery* **2008**, *5*, 593; f) V. Gaberc-Porekar, I. Zore, B. Podobnik, V. Menart, *Curr. Opin. Drug Discovery Dev.* **2008**, *11*, 242.
- [4] a) A. Harada, J. Li, M. Kamachi, *J. Am. Chem. Soc.* **1994**, *116*, 3192; b) F. A. Loiseau, K. K. Hii, A. M. Hill, *J. Org. Chem.* **2004**, *69*, 639; c) S. A. Ahmed, M. Tanaka, *J. Org. Chem.* **2006**, *71*, 9884; d) A. C. French, A. L. Thompson, B. G. Davis, *Angew. Chem., Int. Ed.* **2009**, *48*, 1248; e) G. Székely, M. Schaeperstoens, P. R. Gaffney, A. G. Livingston, *Polym. Chem.* **2014**, *5*, 694; f) A. M. Wawro, T. Muraoka, K. Kinbara, *Polym. Chem.* **2016**, *7*, 2389.
- [5] a) J. V. Jokerst, T. Lobovkina, R. N. Zare, S. S. Gambhir, *Nanomedicine* **2011**, *6*, 715; b) K. Kono, S. Nakashima, D. Kokuryo, I. Aoki, H. Shimomoto, S. Aoshima, K. Maruyama, E. Yuba, C. Kojima, A. Harada, *Biomaterials* **2011**, *32*, 1387; c) Z. Cheng, A. Al Zaki, J. Z. Hui, V. R. Muzykantov, A. Tsourkas, *Science* **2012**, *338*, 903; d) S. Edmonds, A. Volpe, H. Shmeeda, A. C. Parente-Pereira, R. Radia, J. Bagaña-Torres, I. Szanda, G. W. Severin, L. Livieratos, P. J. Blower, *ACS Nano* **2016**, *10*, 10294; e) Y. Cao, J. Yi, X. Yang, L. Liu, C. Yu, Y. Huang, L. Sun, Y. Bao, Y. Li, *Biomacromolecules* **2017**, *18*, 2306; f) Q. Chen, C. Liang, X. Sun, J. Chen, Z. Yang, H. Zhao, L. Feng, Z. Liu, *Proc. Natl. Acad. Sci. U. S. A.* **2017**, *114*, 5343; g) B. Børresen, J. R. Henriksen, G. Clergeaud, J. S. Jørgensen, F. Melander, D. R. Elema, J. Szebeni, S. A. Engelholm, A. T. Kristensen, A. Kjær, *ACS Nano* **2018**, *12*, 11386.
- [6] a) J. Li, Y. Hu, J. Yang, P. Wei, W. Sun, M. Shen, G. Zhang, X. Shi, *Biomaterials* **2015**, *38*, 10; b) R. Lv, P. Yang, F. He, S. Gai, C. Li, Y. Dai, G. Yang, J. Lin, *ACS Nano* **2015**, *9*, 1630; c) X. R. Song, X. Wang, S. X. Yu, J. Cao, S. H. Li, J. Li, G. Liu, H. H. Yang, X. Chen, *Adv. Mater.* **2015**, *27*, 3285; d) S. Bo, Y. Yuan, Y. Chen, Z. Yang, S. Chen, X. Zhou, Z.-X. Jiang, *Chem. Commun.* **2018**, *54*, 3875; e) H. Zhang, S. Chen, Y. Yuan, Y. Li, Z. Jiang, X. Zhou, *ACS Appl. Bio Mater.* **2019**, *2*, 27; f) Y. Zhang, S. Bo, T. Feng, X. Qin, Y. Wan, S. Jiang, C. Li, J. Lin, T. Wang, X. Zhou, Z.-X. Jiang, P. Huang, *Adv. Mater.* **2019**, *31*, 1806444; g) J. Zhu, Y. Xiao, H. Zhang, Y. Li, Y. Yuan, Z. Yang, S. Chen, X. Zheng, X. Zhou, Z.-X. Jiang, *Biomacromolecules* **2019**, *20*, 1281.
- [7] a) T. Sun, Y. S. Zhang, B. Pang, D. C. Hyun, M. Yang, Y. Xia, *Angew. Chem., Int. Ed.* **2014**, *53*, 12320; b) Y. Wang, M. S. Shim, N. S. Levinson, H. W. Sung, Y. Xia, *Adv. Funct. Mater.* **2014**, *24*, 4206; c) W. J. Lokerse, E. C. Kneepkens, T. L. ten Hagen, A. M. Eggermont, H. Grüll, G. A. Koning, *Biomaterials* **2016**, *82*, 138; d) P. Wu, Y. Jia, F. Qu, Y. Sun, P. Wang, K. Zhang, C. Xu, Q. Liu, X. Wang, *ACS Appl. Mater. Interfaces* **2017**, *9*, 25706; e) W. J. Lokerse, A. M. Eggermont, H. Grüll, G. A. Koning, *J. Controlled Release* **2018**, *270*, 282.
- [8] S. Mura, J. Nicolas, P. Couvreur, *Nat. Mater.* **2013**, *12*, 991.
- [9] a) S. Bo, C. Song, Y. Li, W. Yu, S. Chen, X. Zhou, Z. Yang, X. Zheng, Z.-X. Jiang, *J. Org. Chem.* **2015**, *80*, 6360; b) H. Zhang, X. Li, Q. Shi, Y. Li, G. Xia, L. Chen, Z. Yang, Z.-X. Jiang, *Angew. Chem., Int. Ed.* **2015**, *54*, 3763; c) Z. Wan, Y. Li, S. Bo, M. Gao, X. Wang, K. Zeng, X. Tao, X. Li, Z. Yang, Z.-X. Jiang, *Org. Biomol. Chem.* **2016**, *14*, 7912; d) Z. Yu, S. Bo, H. Wang, Y. Li, Z. Yang, Y. Huang, Z.-X. Jiang,

- Mol. Pharmaceutics* **2017**, *14*, 3473; e) T. Deng, X. Mao, Y. Li, S. Bo, Z. Yang, Z.-X. Jiang, *Bioorg. Med. Chem. Lett.* **2018**, *28*, 3502; f) T. Deng, X. Mao, Y. Xiao, Z. Yang, X. Zheng, Z.-X. Jiang, *Bioorg. Med. Chem. Lett.* **2019**, *29*, 581.
- [10] Y. Li, X. Wang, Y. Chen, Z. Yang, Z.-X. Jiang, *Chem. Commun.* **2019**, 55, 1895.
- [11] a) Z.-X. Jiang, Y. Feng, Y. B. Yu, *Chem. Commun.* **2011**, 47, 7233; b) Y. Li, B. Thapa, H. Zhang, X. Li, F. Yu, E.-K. Jeong, Z. Yang, Z.-X. Jiang, *Tetrahedron* **2013**, *69*, 9586.
- [12] Z.-X. Jiang, X. Liu, E.-K. Jeong, Y. B. Yu, *Angew. Chem., Int. Ed.* **2009**, *48*, 4755.
- [13] a) H. Vu-Quang, M. S. Vinding, T. Nielsen, M. G. Ullisch, N. C. Nielsen, J. Kjems, *Nanomed.: Nanotechnol., Biol. Med.* **2016**, *12*, 1873; b) C. Zhang, S. S. Moonshi, W. Wang, H. T. Ta, Y. Han, F. Y. Han, H. Peng, P. Kral, B. E. Rolfe, J. J. Gooding, K. Gaus, A. K. Whittaker, *ACS Nano* **2018**, *12*, 9162; c) O. Munkhbat, M. Canakci, S. Zheng, W. Hu, B. Osborne, A. A. Bogdanov, S. Thayumanavan, *Biomacromolecules* **2019**, *20*, 790.
- [14] J. C. Leroux, *Angew. Chem., Int. Ed.* **2017**, *56*, 15170.